Naval Research Laboratory

Washington, DC 20375-5000

NRL Memorandum Report 6636

Stability Regimes in a Helical Quadrupole Focusing Accelerator—Theory and Simulation

J. KRALL, C. M. TANG, G. JOYCE AND P. SPRANGLE

Beam Physics Branch
Plasma Physics Division

May 4, 1990

REPORT DOCUMENTATION PAGE

Form Approved
OMB No 0704-0188

1. AGENCY USE ONLY *(Leave blank)*	2. REPORT DATE	3. REPORT TYPE AND DATES COVERED
	1990 May 4	Interim

4. TITLE AND SUBTITLE
Stability Regimes in a Helical Quadrupole Focusing Accelerator - Theory and Simulation

5. FUNDING NUMBERS
47-0900-0-0 (JO#)
ARPA Order #4395, A86

6. AUTHOR(S)
J. Krall, C. M. Tang, G. Joyce and P. Sprangle

7. PERFORMING ORGANIZATION NAME(S) AND ADDRESS(ES)
Naval Research Laboratory
Code 4790
Washington, DC 20375-5000

8. PERFORMING ORGANIZATION REPORT NUMBER
NRL Memorandum Report 6636

9. SPONSORING / MONITORING AGENCY NAME(S) AND ADDRESS(ES)
DARPA
Arlington, VA 22209
NSWC
Silver Spring, MD 20903-5000

10. SPONSORING / MONITORING AGENCY REPORT NUMBER

11. SUPPLEMENTARY NOTES

12a. DISTRIBUTION / AVAILABILITY STATEMENT
Approved for public release;
distribution unlimited.

12b. DISTRIBUTION CODE

13. ABSTRACT *(Maximum 200 words)*

The inclusion of helical quadrupole (stellarator) and axial guide fields in high current spiral line or recirculating accelerator configurations provides a high tolerance to energy mismatch and confines the beam against space charge forces. In such a configuration the electron beam can interact with the external fields and with electromagnetic waveguide modes such that the beam centroid can be i) orbit unstable independent of the waveguide modes, ii) three-wave unstable or iii) fully stable. The various stability conditions are presented in the limit of zero beam current. These stability conditions are found to be good predictors of particle simulation results, with minor departures being observed at high current. Linearly unstable modes, obtained via numerical solutions of the dispersion relation, were observed in each simulation. Nonlinear behavior, such as mode saturation in some regimes, was also observed..

14. SUBJECT TERMS		15. NUMBER OF PAGES
High current Accelerator	Strong focusing	29
		16. PRICE CODE

17. SECURITY CLASSIFICATION OF REPORT	18. SECURITY CLASSIFICATION OF THIS PAGE	19. SECURITY CLASSIFICATION OF ABSTRACT	20. LIMITATION OF ABSTRACT
Unclassified	Unclassified	Unclassified	SAR

CONTENTS

STABILITY REGIMES IN A HELICAL QUADRUPOLE FOCUSING ACCELERATOR—THEORY AND SIMULATION

A number of recent high current spiral line or recirculating accelerator configurations utilize strong focusing fields. These fields, consisting of a helical quadrupole field (or stellarator field) and an axial guide field, increase considerably the energy mismatch tolerance of the device and provide confining forces against the beam space charge forces.[1,2] Two such devices are the modified betatron accelerator[3] and the spiral line induction accelerator (SLIA).[4]

The use of strong focusing fields has a potential difficulty in that they can lead to various types of beam instabilities.[5-7] It has been shown that the electron beam centroid can be i) orbit unstable independent of electromagnetic waveguide modes, ii) three-wave unstable or iii) fully stable.[7] Here we present the dispersion relation for the instability and analytic conditions for each of the stability regimes as derived in Ref. 7. Note that the stability conditions are valid only in the limit of zero beam current. Particle simulations in each regime will be presented and compared to both the analytic stability conditions and to numerical solutions of the dispersion relation.

DISPERSION RELATION

We consider an electron beam progagating in an external magnetic field configuration consisting of an axial guide field B_o, and a helical quadrupole field (B_{qx}, B_{qy}),

$$B_{qx} = -B_q k_q (x \sin k_q z - y \cos k_q z), \qquad B_{qy} = B_q k_q (x \cos k_q z + y \sin k_q z), \qquad (1a-b)$$

where $B_q k_q$ is the quadrupole gradient and k_q is the wavenumber of the quadrupole field.

Here we quote the results of Ref. 7, where the wave equation is solved simultaneously with the beam dynamics equation to obtain a dispersion relation. In the analysis it was assumed that: 1) the electron beam propagates within a perfectly conducting cylindrical waveguide of radius r_g (induced image charges and currents were included), 2) the beam radius and beam centroid displacement are small in comparison to the waveguide radius and 3) the electron beam is monoenergetic with velocity v_o and relativistic factor $\gamma_o = (1 - \beta_o^2)^{-1/2}$, where $\beta_o = v_o/c$.

The electromagnetic fields in this case were solved for in terms of right-hand circularly polarized (RHCP) and left-hand circularly polarized (LHCP) waveguide modes. It was

Manuscript approved March 7, 1990.

further assumed that the TE_{11} mode would have the largest growth rate, because it has an electric field that is peaked on axis. The resulting dispersion relation is

$$W_r W_l W_u W_s = k_b^2 \left[(k + k_q - \omega/v_o)^2 D_- W_r + (k - \omega/v_o)^2 D_+ W_l \right], \qquad (2)$$

where $k_b^2 = 2(I_b/17)\mu_{11}^2/(\gamma_o(\mu_{11}^2 r_g^2 - 1)J_1^2(\mu_{11} r_g))$, I_b is the beam current in kA, $\mu_{11} r_g$ is the smallest positive zero of Bessel function J_1', $k = k_+ = k_- - k_q$, $k_\pm$ are the wavenumbers associated with the RHCP and LHCP waves, ω is the radian frequency, $W_r = \omega^2/c^2 - k^2 - \mu_{11}^2$ and $W_l = \omega^2/c^2 - (k + k_q)^2 - \mu_{11}^2$ are contributions from the RHCP and LHCP TE_{11} waveguide modes respectively, $W_s = \bar{K}^2 - (d_1^2 + d_2^2)$ accounts for the two stable beam modes, $W_u = \bar{K}^2 - (d_1^2 - d_2^2)$ admits the two potentially unstable beam modes, $d_1^2 = \bar{K}_2^2 + \bar{K}_1^2/2$, $d_2^2 = \left((\bar{K}_2^2 + \bar{K}_1^2/2)^2 - (\bar{K}_2^4 - \bar{K}_3^4)\right)^{1/2}$, $\bar{K} = k - \omega/v_o + k_q/2$, $\bar{K}_1 = \bar{K}_o - k_q$, $\bar{K}_2^2 = (\bar{K}_o - k_q/2)k_q/2 - k_s^2$, $\bar{K}_3^2 = \bar{K}_q k_q$, $\bar{K}_o = |e|B_o/\beta_o\gamma_o m_o c^2$ is the relativistic cyclotron wavenumber associated with the axial field, $\bar{K}_q = |e|B_q/\beta_o\gamma_o m_o c^2$ is the relativistic cyclotron wavenumber associated with the helical quadrupole field, $k_s = (2(I_b/17)/(\beta_o^2\gamma_o^3 r_g^2))^{1/2}$ and $D_\pm = \bar{K}^2 \mp \bar{K}_1\bar{K} - \bar{K}_2^2$. Equation (2) is mathematically identical to the dispersion relation in Ref. 6 with the vertical field set to zero.

STABILITY REGIMES

The dispersion relation, Eq. (2), contains i) a region of orbital instability, ii) two regions of three-wave instability and iii) two regions of stability. The stability conditions were obtained from the dispersion relation in the limit of zero beam current.[7] They delineate stable and unstable regions of $(k_q, \bar{K}_o)$ space for given values of γ, r_g and $B_q k_q$.

i) Orbit Unstable Regime

The electron beeam is both orbit and three-wave unstable when $(d_1^2 - d_2^2) \leq 0$, which gives the unstable values of $\bar{K}_o$:

$$\bar{K}_{crit,2} \equiv k_q/2 - 2\bar{K}_q \leq \bar{K}_o \leq \bar{K}_{crit,3} \equiv k_q/2 + 2\bar{K}_q. \qquad (3)$$

ii) Three-Wave Unstable Regimes

Numerical solutions of the dispersion relation (2) indicate that the three-wave instability occurs when the RHCP waveguide mode [or the LHCP waveguide mode] intersects, in the (ω, k) plane, the appropriate beam mode given by $W_u = 0$ and $(d_1^2 - d_2^2) > 0$. For $K_o < K_{crit,2}$, the three-wave interaction is unstable (Region I) when the RHCP waveguide mode intersects the beam line $\omega/v_o = (k + k_q/2) + \sqrt{d_1^2 - d_2^2}$ $\simeq k + k_q$ (for $K_o \geq 0$) or $\simeq k + k_q - K_o$ (for $0 < K_o < K_{crit,2}$). For $K_o > K_{crit,3}$, the three-wave interaction is unstable (Region II) when the RHCP waveguide mode intersects the beam line $\omega/v_o = (k + k_q/2) - \sqrt{d_1^2 - d_2^2} \simeq k + K_o$. The two three-wave unstable regimes are those portions of (k_q, K_o) parameter space that do not satisfy the stability conditions below. Note that while the three-wave instability is present in the orbit-unstable regime, the orbit instability dominates in that regime.

iii) Three-Wave Stable Regime for $K_o < K_{crit,2}$

Stability is achieved when the waveguide cut-off frequency $\mu_{11}c$ is sufficiently large that intersection with either of the beam lines, defined by $W_u = 0$ cannot be achieved. For $K_o < K_{crit,2}$, the beam is stable if

$$q\mu_{11} \geq k_q + 2\left(d_1^2 - d_2^2\right)^{1/2}, \tag{4}$$

where $q = \left(4/(\gamma_o^2 - 2)\right)^{1/2}$. For $k_q < q\mu_{11}$, and defining $\zeta = k_q^2(1 + 8K_q^2/f) - 2f$ and $f = q\mu_{11}(k_q - q\mu_{11}/2)$, the electron beam is stable for the following situations:

a) for $f > 0$ and $\zeta > 0$, the stable range of K_o is given by

$$K_{crit,1} \equiv k_q/2 - \zeta^{1/2}/2 < K_o < K_{crit,2}, \tag{5a}$$

b) for $f < 0$ and $\zeta > 0$, the stable values of K_o are

$$K_o < smaller\ \ of\,(K_{crit,1}, K_{crit,2}), \tag{5b}$$

c) for $f < 0$ and $\zeta < 0$, all values of $K_o < K_{crit,2}$ are stable.

iv) Three-Wave Stable Regime for $K_o > K_{crit,3}$

The three-wave interaction is also stable when the RHCP waveguide mode does not intersect the beam line $\omega/v_o = (k + k_q/2) - \sqrt{d_1^2 - d_2^2}$ for $K_o > K_{crit,3}$. This occurs when $q\mu_{11} \geq k_q - 2\left(d_1^2 - d_2^2\right)^{1/2}$, for which there are two stable cases:

a) for $k_q < q\mu_{11}$, the stable range of K_o is

$$K_o > K_{crit,3}, \tag{6a}$$

b) for $k_q > q\mu_{11}$, the stable range of K_o is

$$K_o > K_{crit,4} \equiv k_q/2 + \zeta^{1/2}/2. \tag{6b}$$

In the limit of small quadrupole gradient, large γ_o and $K_o > K_{crit,3}$, the stability condition[8] is approximately $K_o > k_q - \mu_{11}/\gamma_o$.

The various operating regimes are illustrated as functions of k_q and B_o in Fig. 1, for $\gamma_o = 7$, $r_g = 3\ cm$ and quadrupole gradient $B_q k_q = 200\ G/cm$. Since the stability boundaries are obtained in the limit of zero beam current, the area of the two stable regions will shrink slightly as the current is increased.

It is clear from the analysis that the value of $B_o > 0$ required for stability increases with beam energy. To operate in the stable regime with a fixed value of $B_o > 0$, both the maximum allowable quadrupole gradient and the quadrupole wavenumber must decrease for increasing beam energy. Figure 2 is a plot of maximum quadrupole gradient versus γ_o for a fixed guide field $B_o = 5\ kG$, $r_g = 3\ cm$ and two different values of quadrupole wavenumber: $k_q = 0.1\ cm^{-1}$ (—) and $k_q = 0.05\ cm^{-1}$(- - -).

NUMERICAL RESULTS

For the present numerical study we use the ELBA[9] code, a three-dimensional particle code which simulates a beam propagating within a cylindrical metallic pipe. The full set of Maxwell's equations along with the full relativistic motion of the beam particles are included. The initial beam parameters, calculated by the STELMAT[10] code, are matched to the field configuration to minimize initial oscillations. The ELBA code contains numerous beam diagnostics. These include an emittance diagnostic[11] that was developed for beams with x-y coupling.

Growth rates were measured by analyzing the TE_{11} mode, for which the B_z and E_r components may be "projected out" from the electromagnetic spectrum in a straightforward manner. The growth rate is then obtained as a function of ω and k for those cases in

which an unstable mode grew above the background "noise". Because our simulation takes place in a coordinate system that moves with the beam ($r, \theta, \zeta = ct - z$), these growth rates are $\Gamma/c = Im(\omega/c - k)$. This corresponds to the theoretical result only in the case that $Im(k) = 0$ as was assumed in numerically solving the dispersion relation (2).

Simulations have been performed for parameters typical of a high current beam, $I_b = 10\ kA$, $\gamma_o = 7$ and normalized RMS emittance, $\epsilon_{n,rms} = .158\ cm - rad$. We fixed the waveguide radius at $r_g = 3\ cm$ and the quadrupole gradient at $B_q k_q = 200\ G/cm$. In a typical run, a 1 meter beam was transported over 10 meters in the presence of the external focusing fields. For these runs, we set $k_q = 0.5\ cm^{-1}$ and varied B_o so as to sample each of the unstable regions and the larger of the two stable regions of the stability diagram (Fig. 1). The smaller stable region with $B_o < 0$ was considered by setting $k_q = 0.09\ cm^{-1}$. The (k_q, B_o) location of each simulation is indicated in Fig. 1. We found stable behavior in the analytically stable regions and physically distinct behavior in each of the unstable regions. Numerical results $(\Gamma/c, \omega/c, k)$ are sumarized in Table 1 for the $k_q = 0.5\ cm^{-1}$ runs. Theoretical values, from numerical solutions of the dispersion relation, are also given.

Simulations in unstable region I were performed with $B_o = 0$, 1 and 2 kG. The beam centroid (x-component) and beam envelope (major and minor radii of the beam cross section) are plotted versus time for a fixed position within the beam in Fig. 3 for the $B_o = 1\ kG$ case. Here, the beam develops a macroscopic transverse motion, qualitatively similar to that assumed in the analytical model (pencil beam, rigid displacements). In fact, the wavenumber of the beam centroid motion for each of these runs matched the linear theory within 5%. When the transverse displacement reaches its peak (saturated) value, the cross-sectional area and emittance of the beam increase and current loss sets in. This was also observed in the $B_o = 2\ kG$ case, where saturation occurs at a displacement of $\simeq 0.1\ cm$ after 8 meters of propagation and is followed by a steady loss of current and rise in emittance. Complete saturation was not observed in the $B_o = 0$ case within the length of the simulation. The Fourier spectrum of the B_z component of the TE_{11} mode for the $B_o = 1\ kG$ run is plotted versus k in Fig. 4 and compares favorably to the growth rate versus k plotted in Fig. 5.

In unstable region II, we found saturation of the instability with displacements in the

1 to 2 mm range without loss of current or growth in emittance. Such runs were performed at $B_o = 4.5,\ 4.75$ and $5.0\ kG$. Plots of beam centroid (x-component) and beam envelope are shown in Fig. 6 for the $B_o = 5\ kG$ case. The Fourier spectrum of the B_z component of the TE_{11} mode at $ct = 600\ cm$ is plotted in Fig 7 and compares favorably to the plot of Γ/c versus k from the dispersion relation (Fig. 8). Figure 9 shows the growth and decay of the linear component of the mode at $k = 1.5\ cm^{-1}$. Higher wavenumber modes are also in evidence but are within the range of unstable wavenumbers predicted by the linear theory. In the $B_o = 4.5$ and $4.75\ kG$ cases, higher wavenumber modes appeared that were outside the linear range of instability, suggesting that higher order linear or nonlinear modes had been excited. Note that in the 5 kG case the dispersion relation gives nonzero growth rates for $0.6 < k < 3.0\ cm^{-1}$ and for $5.7 < k < 9\ cm^{-1}$. Our numerical parameters were such that wavenumbers in the higher range were not properly resolved.

Simulations of orbit-unstable configurations were performed at $B_o = 4.0$ and $4.3\ kG$. These points in parameter space reside in an orbit-stable region of the stability diagram, but are revealed to be orbit unstable when the disperison relation is solved numerically. This is indicated in Fig. 10, where Γ versus k is plotted for $B_o = 4.3\ kG$. In each of the two simulations, the major radius of the beam expanded to make contact with the wall within less than 1 meter of propagation, resulting in a severe loss of beam current.

Runs were also performed in each of the two stable regimes, at $k_q = 0.5$, $B_o = 6.0\ kG$ and at $k_q = 0.09$, $B_o = -4\ kG$. No indication of instability was observed in either case.

DISCUSSION

Two items among the results above deserve comment. These are 1) the observed saturation without current loss in three-wave unstable regime II and 2) the extension of the orbit instability into three-wave unstable region II at high current.

The saturation of the instability in three-wave unstable regime II without emittance growth or current loss is not well-understood. Unstable region II differs from unstable region I in that the instability occurs at higher wavenumbers and with a larger bandwidth, which may allow the possiblity of mode competition as the instability develops. Also, at short wavelengths, a moderate spread in the parallel energy of the beam may disrupt the instability. This saturation mechanism was suggested in Ref. 8. Because the group

velocity of the TE_{11} mode is close to c in this regime, it is possible that an electron trapping mechanism could cause saturation, but the multiple wavenumbers observed both in the radiation field and in the beam centroid motion make this unlikely. It was not clear from either the analysis or the simulations which, if any, of these phenomena are responsible for the observed saturation.

The analysis of the dispersion relation suggests that the orbit instability is centered on a region of parameter space where the cyclotron wavenumber, K_o, is approximately equal to $k_q/2$ [see Eq. (3)]. For such values, a particle gyrating around the axis experiences a constant radial force from the quadrupole fields, i.e., $\Gamma(k = 0) \neq 0$. At high current, however, the bandwidth of the instability in three-wave unstable region II widens to encompass $k = 0$ for parameters which lie outside the orbit-unstable regime in the stability diagram of Fig. 1 (recall that the stability diagram is correct only as $I_b \rightarrow 0$). This effect can occur in three-wave unstable region I, but is less significant because of the narrow unstable bandwidth in that region. In fact, the unstable region expands from $2.2 < B_o < 3.8\ kG$, as suggested by the stability diagram, to $2.2 < B_o < 4.3\ kG$ (see Fig. 10). This extension of the orbit unstable regime into three-wave unstable region II is the only significant departure from the stability diagram at high current.

CONCLUSIONS

In this study, we have used electromagnetic particle simulation to examine the physics of the three-wave instability. We first presented the dispersion relation of Ref. 7 for transverse oscillations of an electron beam propagating within a drift tube in the presence of external solenoidal and helical quadrupole focusing fields. We also presented analytic stability conditions from this dispersion relation in the limit of zero beam current and have found that these stability conditions are good predictors of particle simulation results, even at currents as high as 10 kA. In accordance with the theory, we find that as we vary the external field parameters, the simulations show two stable regimes of beam propagation, two three-wave unstable regimes and an orbit-unstable regime. The only significant departure from the stability conditions at these high currents had the effect of extending the orbit instability into three-wave unstable regime II. Numerical solutions of the dispersion relation were found to be in qualitative agreement with particle simulation results in all

cases, although the simulations gave lower growth rates in many cases. Additionally, we have observed saturation of the instability in both three-wave unstable regimes. This was associated with emittance growth and the onset of beam loss in three-wave unstable region I, but was without these effects in unstable region II. The saturation mechanism in the latter case is not clear, but may be related to the short wavelengths, wide bandwidths and possible mode competition which occur in three-wave unstable region II, but are absent in region I.

Acknowledgments

This work was supported by Defense Advanced Research Projects Agency, ARPA Order No. 4395, Amendment 80, monitored by Naval Surface Warfare Center. We would also like to thank D. Chernin and A. Mondelli for their insight and T. Swyden for his assistance.

REFERENCES

1. C. W. Roberson, A. Mondelli and D. Chernin, Phys. Rev. Lett. 50, 507 (1983).
2. P. Sprangle and C. A. Kapetanakos, Part. Accel. 18, 203 (1986).
3. J. Golden, J. Pasour, D. E. Pershing, T. Smith, F. Mako, S. Slinker, F. Moro, N. Orrick, R. Altes, A. Fliflet, P. Champney and C. A. Kapetanakos, IEEE Trans. on Nucl. Sci. NS-30, 2114 (1983).
4. A. Mondelli, D. Chernin, S. D. Putnam, L. Schlitt and V. Bailey, Proc. Sixth Intl. Conf. on High Power Part. Beams (Osaka, Japan), (1986); V. Bailey, L. Schlitt, M. Tiefenback, S. Putnam, A. Mondelli, D. Chernin and J. Petillo, Proc. of the 1987 IEEE Particle Accel. Conf., 920 (1987).
5. B. Levush, T. M. Antonsen, W. M. Manheimer and P. Sprangle, Phys. Fluids 28, 7 (1985).
6. T. P. Hughes and B. B. Godfrey, Phys. Fluids 29, 1698 (1986).
7. C. M. Tang, P. Sprangle, J. Krall, P. Serafim and F. Mako, submitted to Part. Accel.
8. D. Chernin and T. Hughes (private communication).
9. G. Joyce, J. Krall and S. Slinker, Proc. of the Conf. on Computer Codes and the Linear Accel. Community (to be published by AIP), (1990).
10. D. Chernin (private communication).
11. D. Chernin, Part. Accel. 24, 29 (1988).

Table 1

	THEORY			SIMULATION		
$B_o(kG)$	Γ/c	ω/c	k	Γ/c	ω/c	k
0	0.031	0.71	0.24	0.005	0.64	0.17
1.0	0.033	0.78	0.38	0.015	0.76	0.37
2.0	0.043	1.03	0.72	0.033	0.81	0.49
4.0	orbit-unstable			orbit-unstable		
4.3	orbit-unstable			orbit-unstable		
4.5	0.023	0.98	0.82	0.025	1.06	0.81
4.75	0.016	1.29	1.16	0.013	1.06	1.09
5.0	0.012	1.74	1.65	0.011	1.87	1.50
6.0	stable			stable		

Theoretical values of $(\omega/c, k)$ for modes with peak linear growth rates, Γ/c, and corresponding *numerical* values for these unstable modes. Growth rates, frequencies and wavenumbers are in units of cm^{-1}. Note that for cases where multiple unstable modes were observed (B_o = 4.5, 4.75 and 5 kG), only the mode corresponding to the linear growth rate was reported.

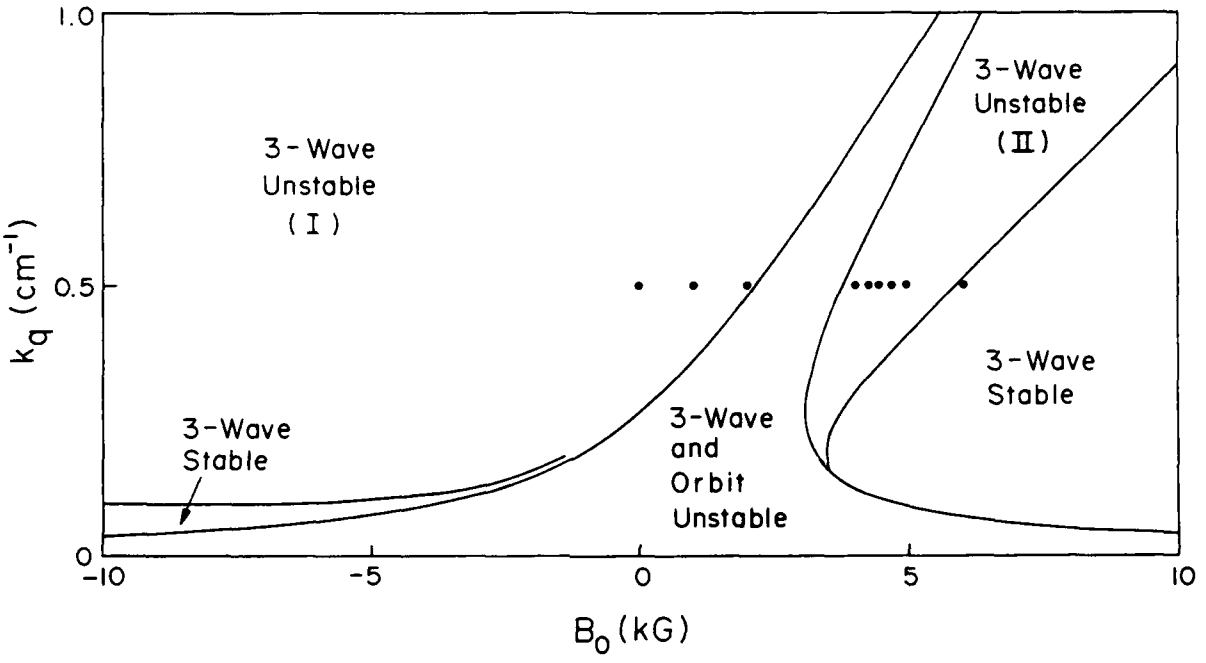

Fig. 1. Plot of the various operating regimes for $\gamma_o = 7$, $r_g = 3\ cm$ and quadrupole gradient $B_q k_q = 200\ G/cm$.

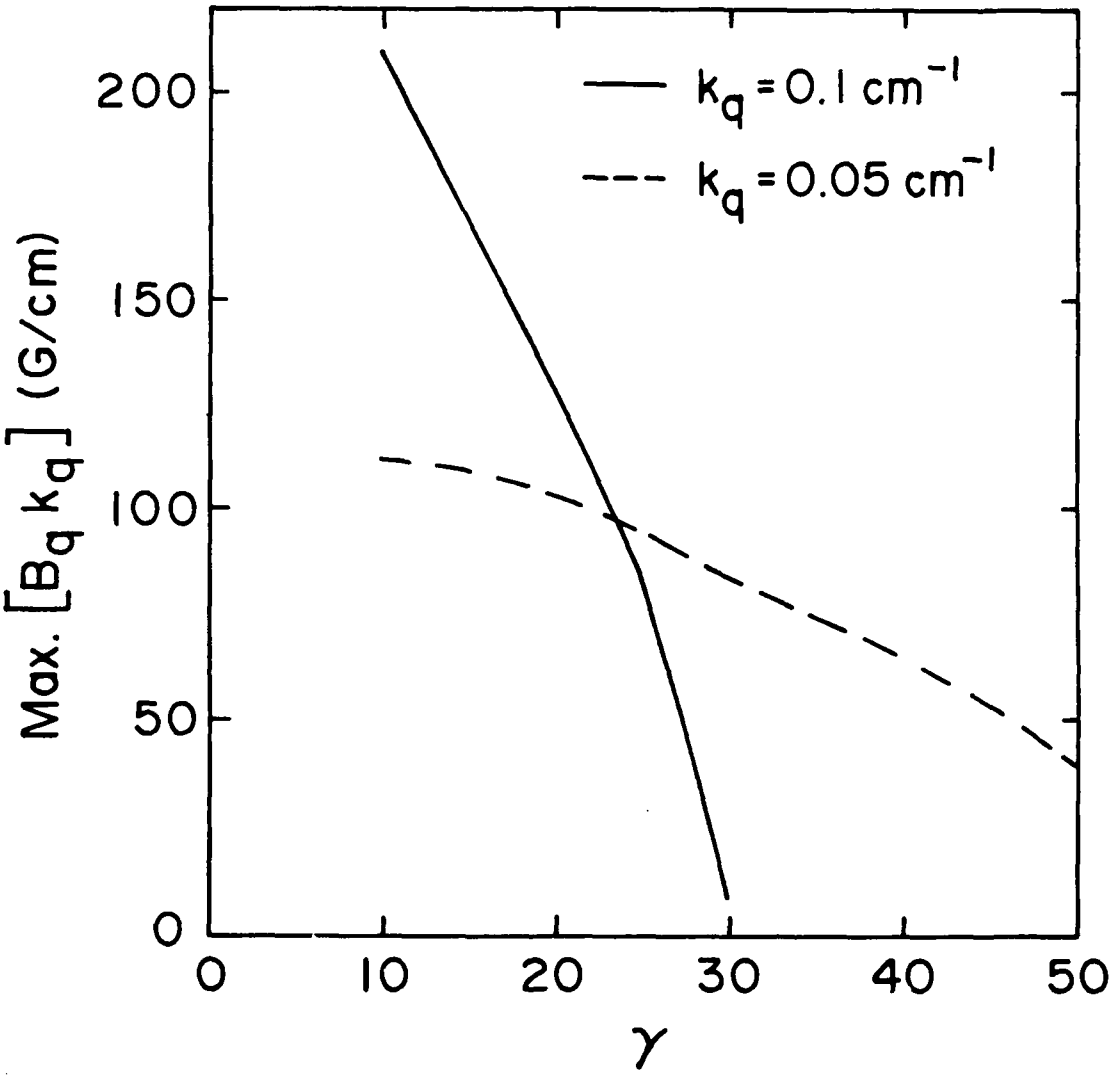

Fig. 2. Plot of maximum quadrupole gradient versus γ_o for guide field $B_o = 5\ kG$ and $r_g = 3\ cm$.

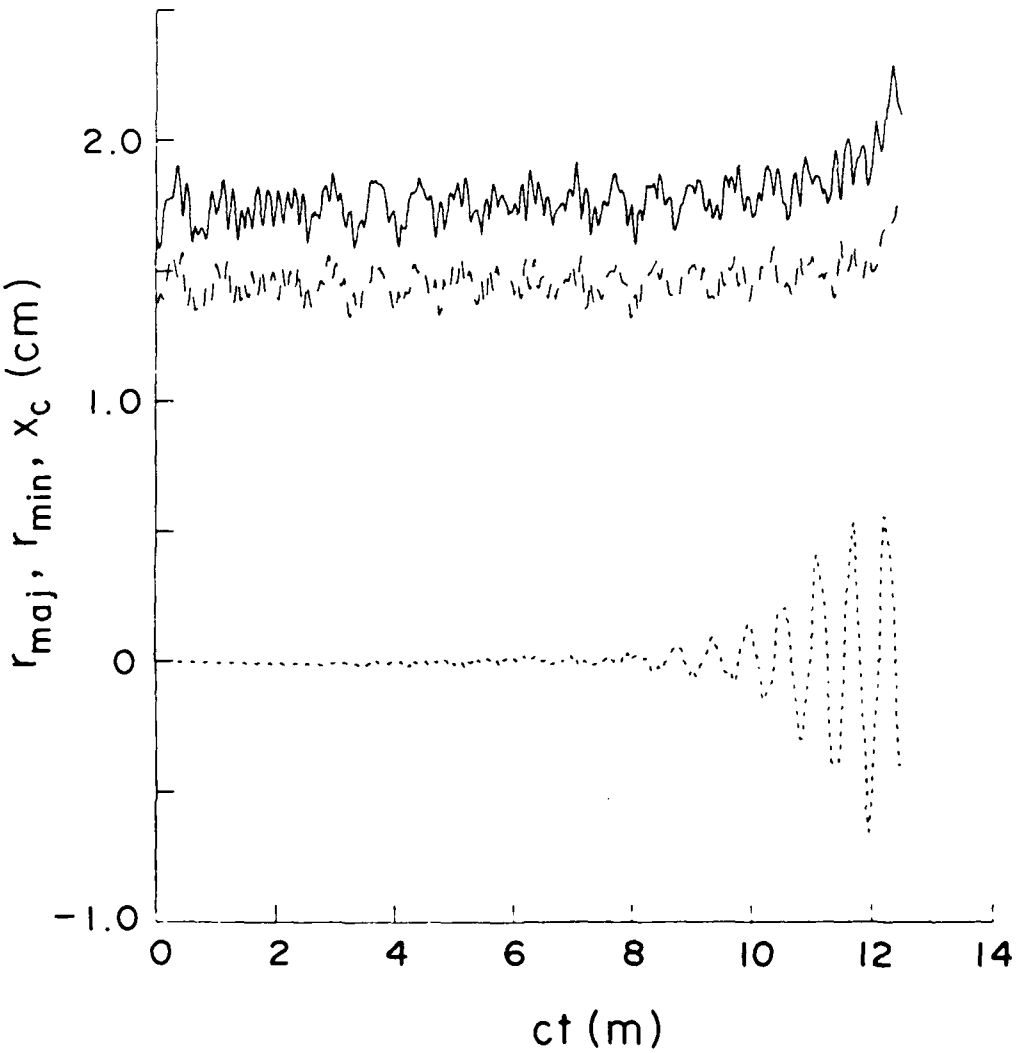

Fig. 3. The major radius of the beam cross section (solid line), the minor radius (dashed line) and the beam centroid x-component (dotted line) are plotted versus time for the $B_o = 1\ kG$ case.

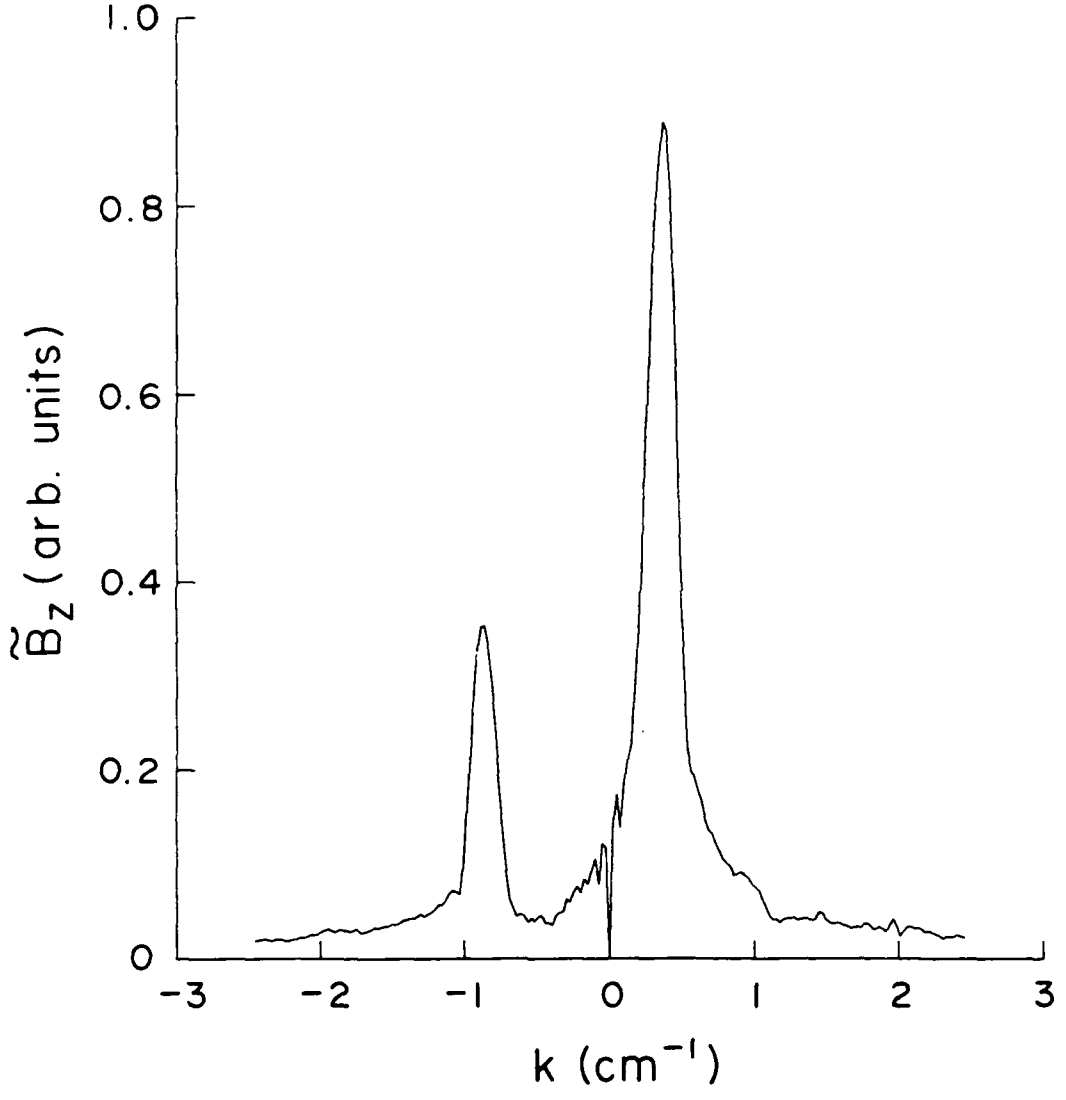

Fig. 4. The Fourier spectrum of the B_z component of the TE_{11} mode is plotted versus k for the $B_o = 1\ kG$ case.

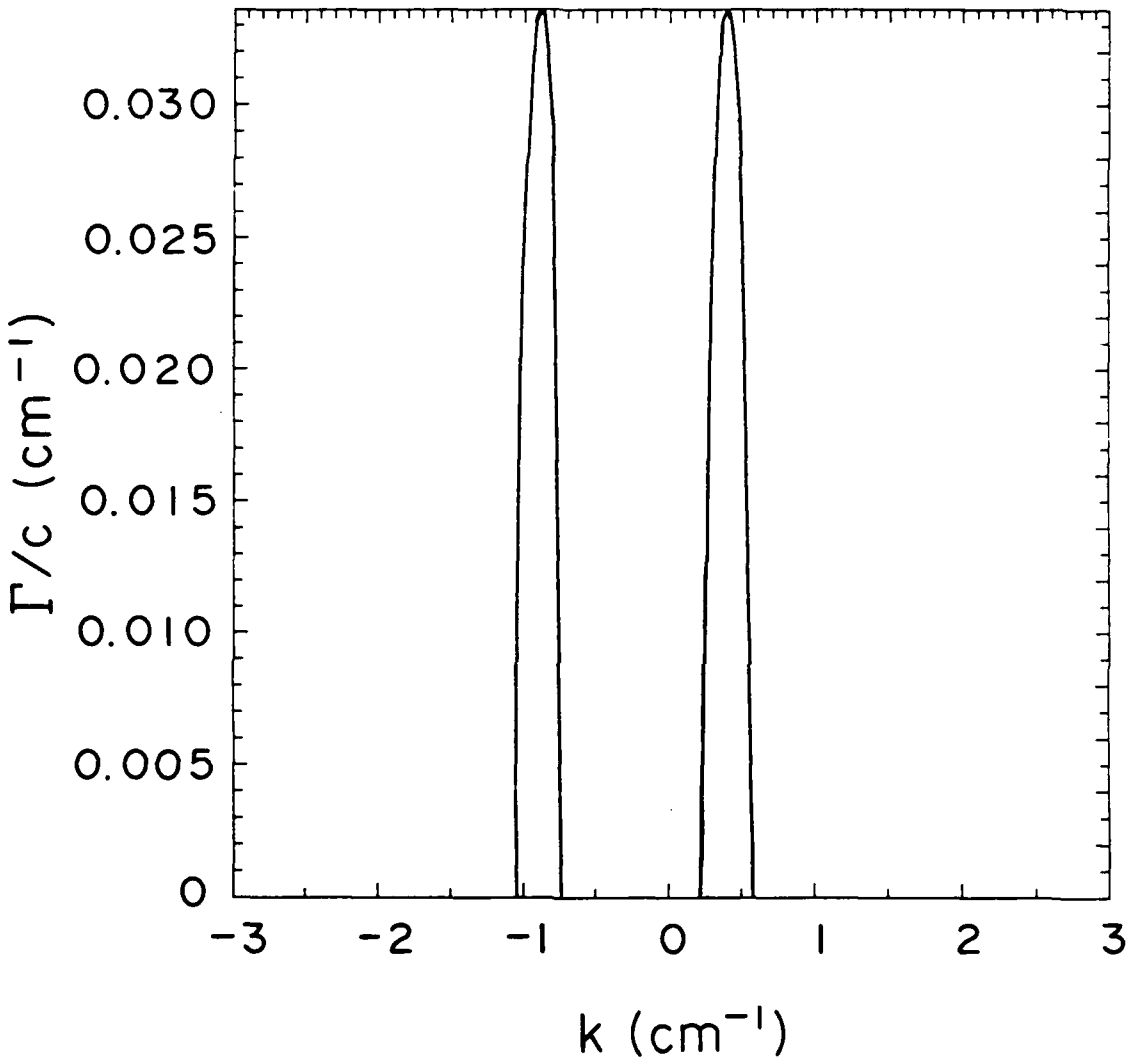

Fig. 5. The temporal growth rate, as calculated from the dispersion relation, is plotted versus k for the $B_o = 1\ kG$ case.

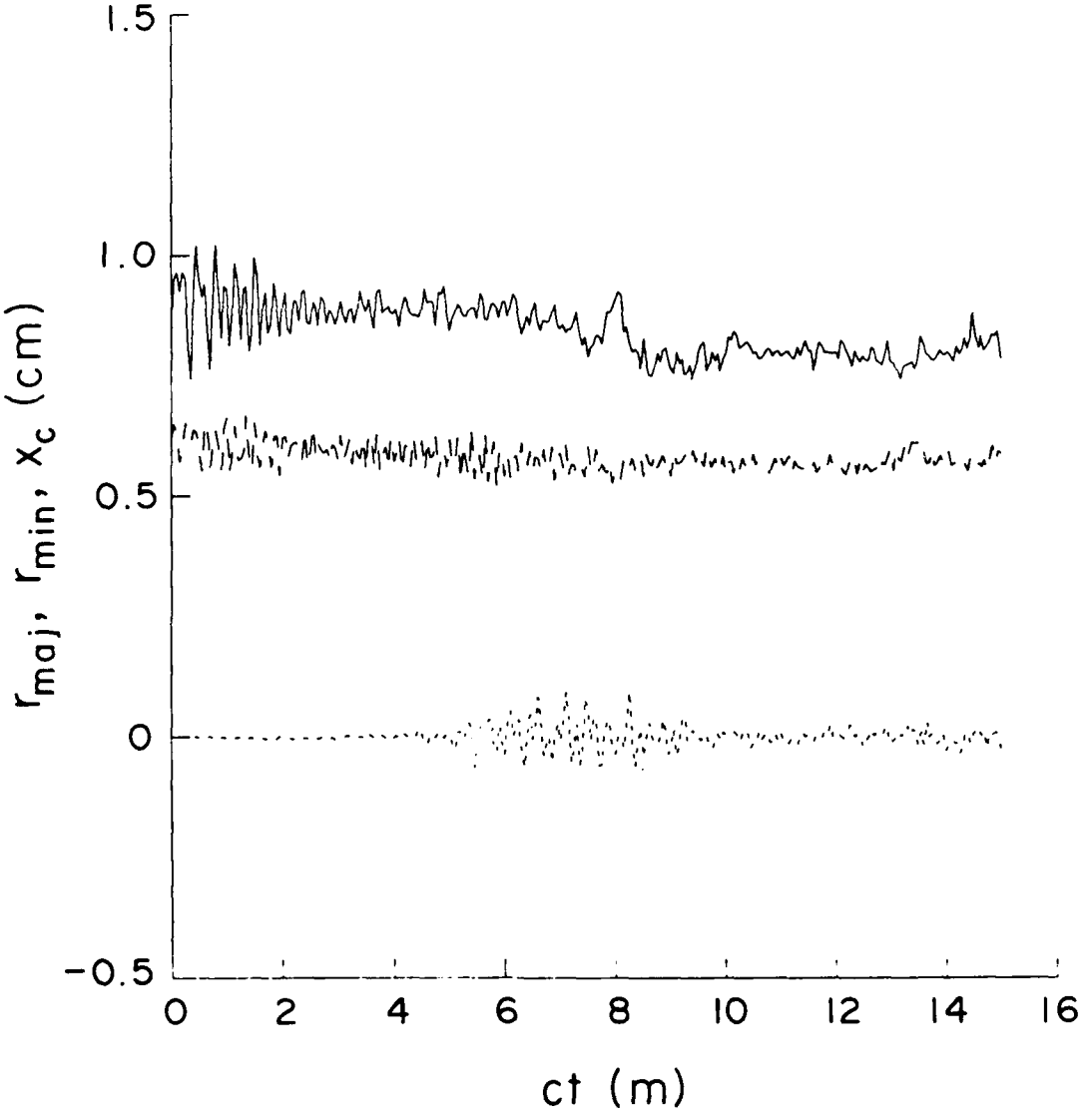

Fig. 6. The major radius of the beam cross section (solid line), the minor radius (dashed line) and the beam centroid x-component (dotted line) are plotted versus time for the $B_o = 5\ kG$ case.

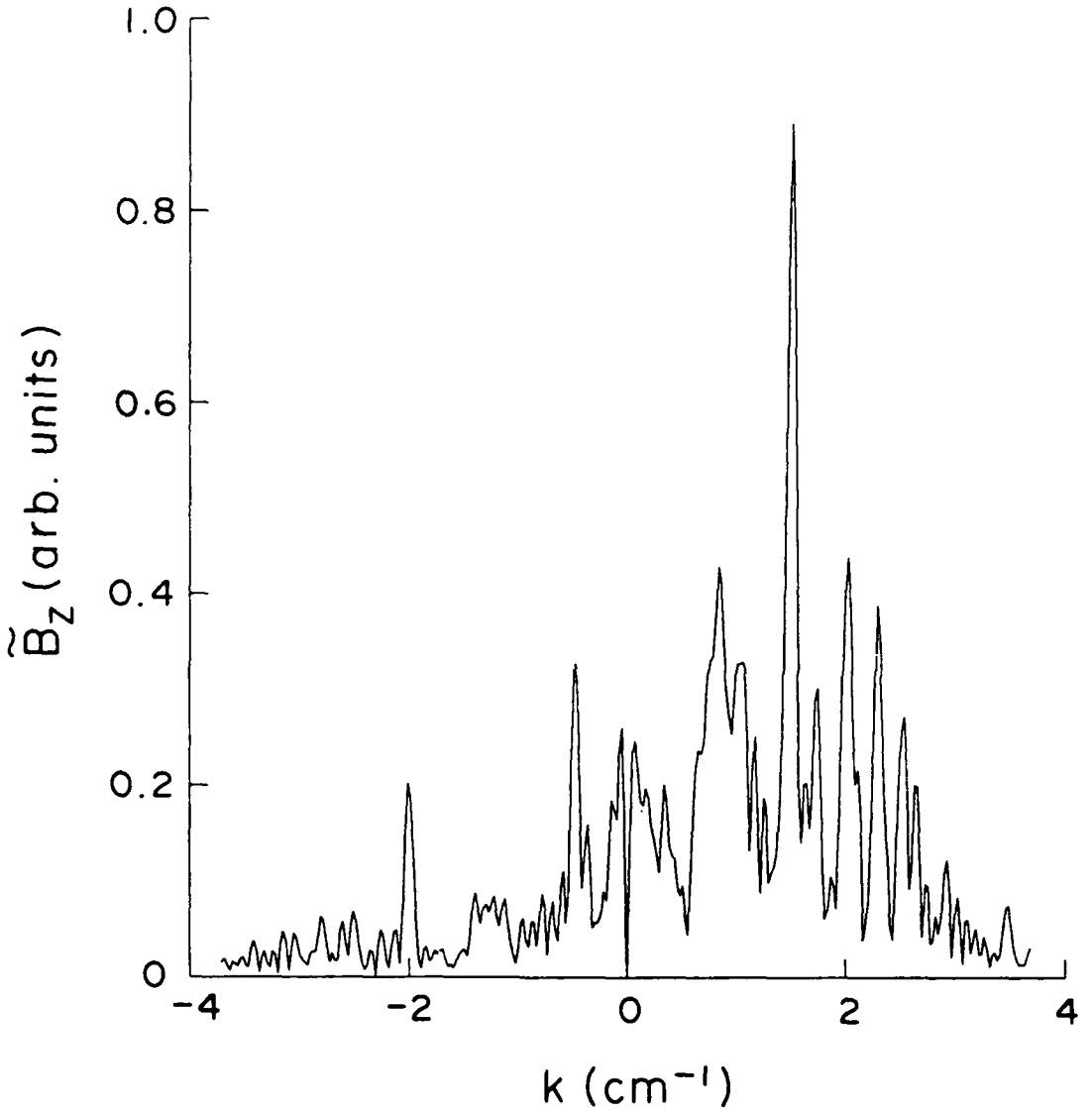

Fig. 7. The Fourier spectrum of the B_z component of the TE_{11} mode is plotted versus k for the $B_o = 5\ kG$ case.

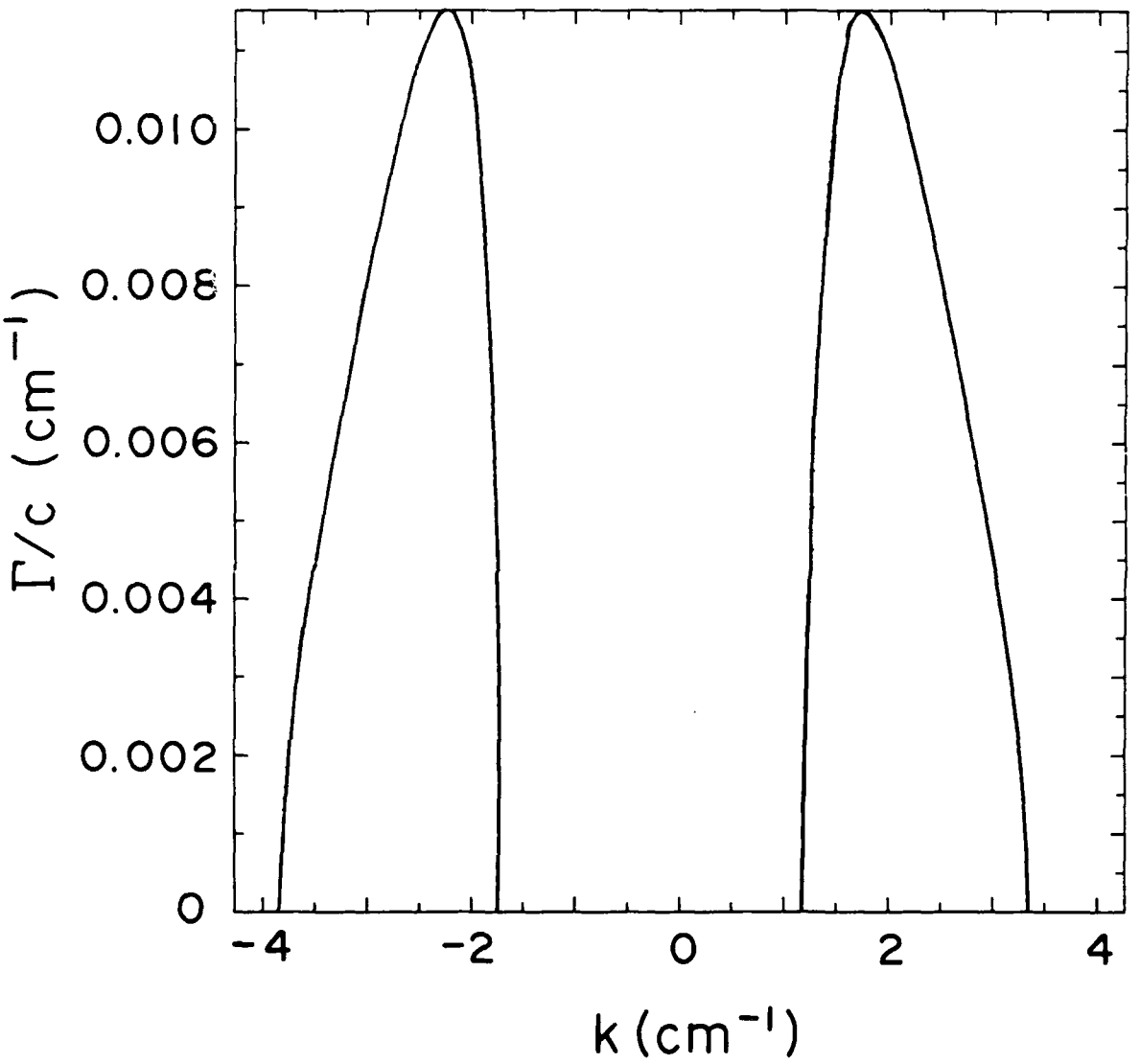

Fig. 8. The temporal growth rate, as calculated from the dispersion relation, is plotted versus k for the $B_o = 5\ kG$ case.

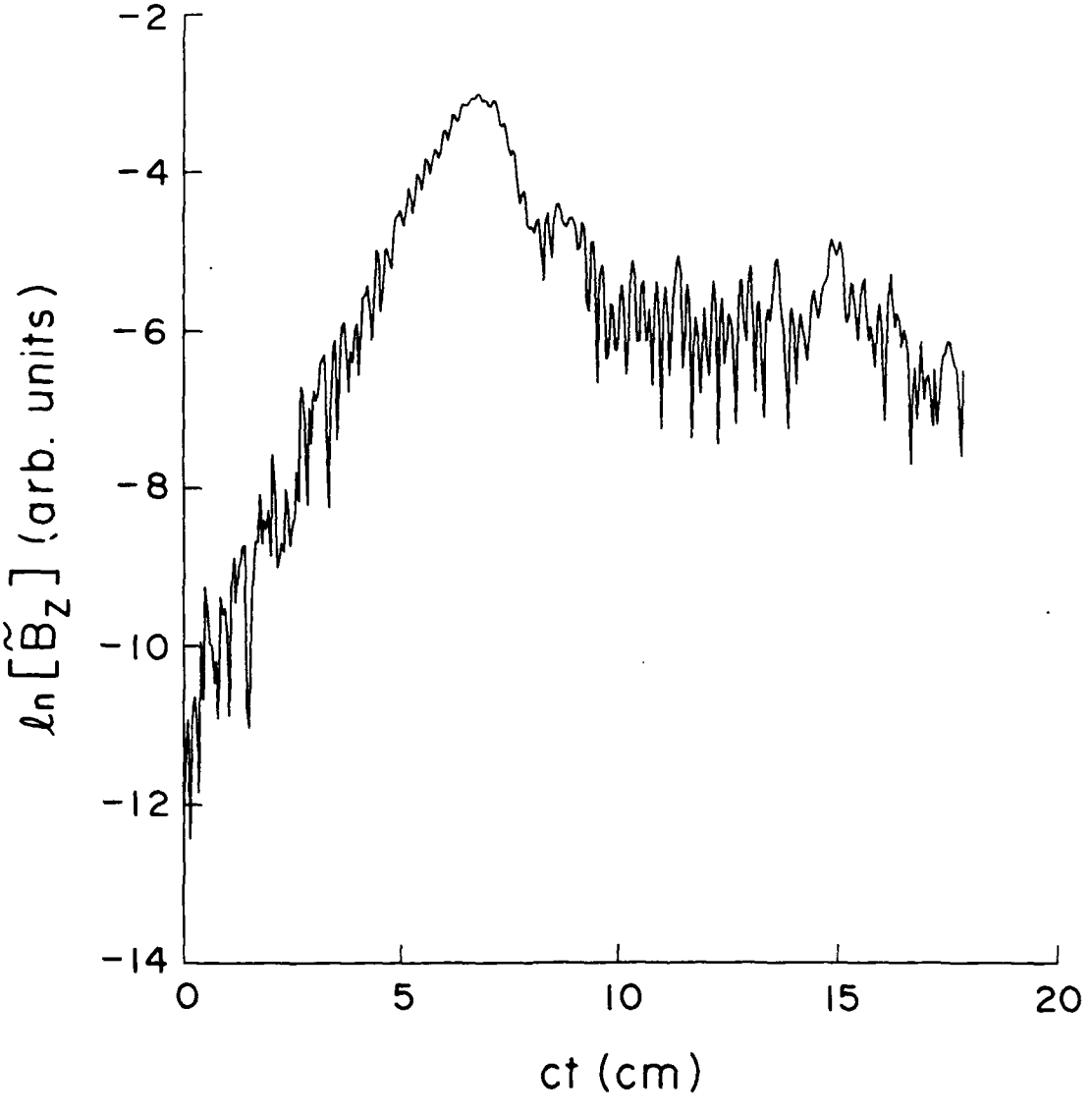

Fig. 9. Fourier component of $B_z(k = 1.5\ cm^{-1})$ of the TE_{11} mode versus time.

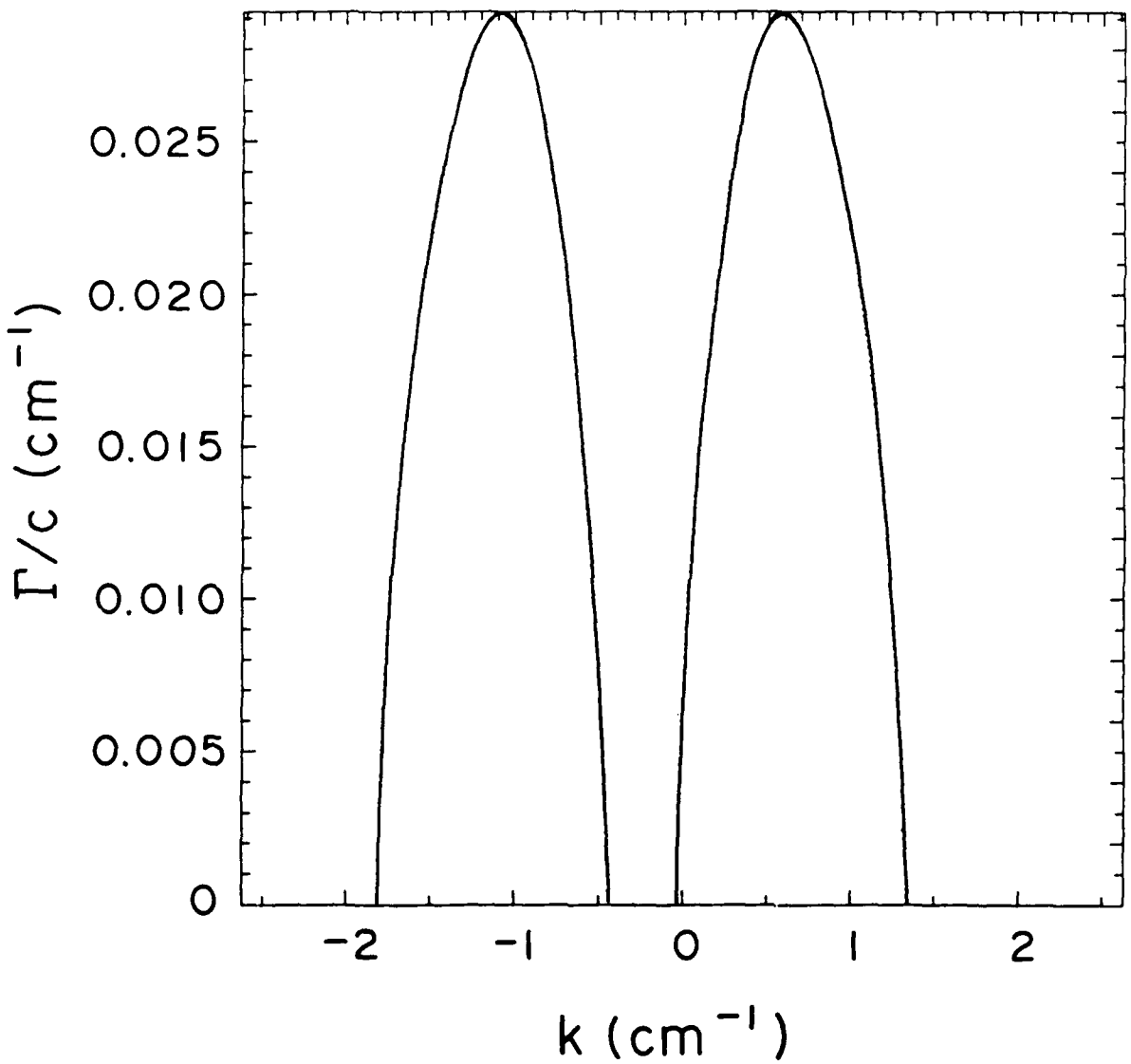

Fig. 10. Growth rate versus k for the $k_q = 0.5$, $B_o = 4.3\ kG$ case. A nonzero growth rate at k = 0 indicates orbit instability.

Distribution List

Naval Research Laboratory
4555 Overlook Avenue, S.W.
Attn: CAPT J. J. Donegan, Jr. - Code 1000
Dr. M. Lampe - Code 4792
Dr. T. Coffey - Code 1001
Head, Office of Management & Admin - Code 1005
Deputy Head, Office of Management & Admin - Code 1005.1
Directives Staff, Office of Management & Admin - Code 1005.6
Director of Technical Services - Code 2000
ONR - Code 0124
NRL Historian - Code 2604
Dr. W. Ellis - Code 4000
Dr. J. Boris - Code 4040
Dr. M. Picone - Code 4040
Dr. M. Rosen - Code 4650
Dr. M. Haftel - Code 4665
Dr. S. Ossakow - Code 4700 (26 copies)
Dr. A. Robson - Code 4708
Dr. M. Friedman - Code 4750
Dr. R. Meger - Code 4750
Dr. J. Antoniades - Code 4751
Dr. T. Peyser - Code 4751
Dr. D. Murphy - Code 4751
Dr. R. Pechacek - Code 4750.1
Dr. G. Cooperstein - Code 4770
Dr. A. Ali - Code 4780
Dr. D. Colombant - Code 4790
Dr. R. Fernsler - Code 4790
Dr. I. Haber - Code 4790
Dr. R. F. Hubbard - Code 4790
Dr. G. Joyce - Code 4790 (20 copies)
Dr. Y. Lau - Code 4790
Dr. S. P. Slinker - Code 4790
Dr. P. Sprangle - Code 4790 (20 copies)
Dr. C. M. Tang - Code 4790 (20 copies)
Dr. E. Esarey - Code 4790
Dr. T. Godlove - Code 4790
Dr. J. Marsh - Code 4790
Dr. Y. H. Seo - Code 4790
Dr. R. Taylor - Code 4790
Dr. J. Krall - Code 4790 (20 copies)
B. Pitcher - Code 4790A
Mr. P. Boris - SAIC (Code 4790)
Dr. S. Gold - Code 4793
Dr. C. Kapetanakos - Code 4795
Library - Code 2628 (22 copies)
D. Wilbanks - Code 2634
Code 1220

Air Force Office of Scientific Research
Physical and Geophysical Sciences
Bolling Air Force Base
Washington, DC 20332
Attn: Major Bruce Smith

Air Force Weapons Laboratory
Kirtland Air Force Base
Albuquerque, NM 87117-6008
Attn: William L. Baker (AFWL/NTYP)
Breddan B. Godfrey

U. S. Army Ballistics Research Laboratory
Aberdeen Proving Ground, Maryland 21005
Attn: Dr. Donald Eccleshall (DRXBR-BM)
Dr. Anand Prakash
Dr. Clinton Hollandsworth

Ballistic Missile Def. Ad. Tech. Ctr.
P.O. Box 1500
Huntsville, Alabama 35807
Attn: Dr. M. Hawie (BMDSATC-1)

Chief of Naval Material
Office of Naval Technology
MAT-0712, Room 503
800 North Quincy Street
Arlington, VA 22217
Attn: Dr. Eli Zimet

Commander
Space and Naval Warfare Systems Command
National Center 1, Room 8E08
Washington, DC 20363-5100
Attn: RADM Robert L. Topping

Cornell University
369 Upson Hall
Ithaca, NY 14853
Attn: Prof. David Hammer

Defense Advanced Research Projects Agency
1400 Wilson Blvd.
Arlington, VA 22209
Attn: Dr. H. L. Buchanan
Dr. B. Hui

Defense Nuclear Agency
Washington, DC 20305
Attn: Dr. Muhammad Owais (RAAE)

Department of Energy
Washington, DC 20545
Attn: Dr. Wilmot Hess (ER20:GTN,
High Energy and Nuclear Physics)
Mr. Gerald J. Peters (G-256)

Directed Technologies, Inc.
1500 Wilson Blvd. Suite 515
Arlington, VA 22209
Attn: Mr. Ira F. Kuhn
Dr. Nancy Chesser

HQ Foreign Technology Division
Wright-Patterson AFB, OH 45433
Attn: TUTD/Dr. C. Joseph Butler

Institute for Defense Analyses
1801 N. Beauregard Street
Alexandria, VA 22311
Attn: Dr. Deborah Levin
Ms. M. Smith

JAYCOR
11011 Torreyana Road
P. O. Box 85154
San Diego, CA 92138-9259
Attn: Dr. Franklin S. Felber
Dr. Seung Kai Wong

JAYCOR
39650 Libery Street, Suite 320
Freemont, CA 94538
Attn: Dr. Kendal Casey

Joint Institute for Laboratory
Astrophysics
National Bureau of Standards and
University of Colorado
Boulder, CO 80309
Attn: Dr. Arthur V. Phelps

Kaman Sciences
P. O. Drawer QQ
Santa Barbara, CA 93102
Attn: Dr. W. Hobbs

La Jolla Institute
P. O. Box 1434
La Jolla, CA 92038
Attn: Dr. K. Brueckner

Lawrence Berkeley Laboratory
University of California
Berkeley, CA 94720
Attn: Dr. Edward P. Lee
Dr. Thomas Fessenden

Lawrence Livermore National Laboratory
University of California
Livermore, California 94550
Attn: Dr. Simon S. Yu
Dr. Frank Chambers
Dr. James W.-K. Mark, L-477
Dr. William Fawley
Dr. William Barletta
Dr. William Sharp
Dr. Daniel S. Prono
Dr. John K. Boyd
Dr. John Clark
Dr. George J. Caporaso
Dr. Donald Prosnitz
Dr. John Stewart
Dr. Y. P. Chong
Major Kenneth Dreyer
Dr. Hans Kruger
Dr. Thaddeus J. Orzechowski
Dr. Michael R. Teague
Mr. John T. Weir

Dr. James E. Leiss
13013 Chestnut Oak Drive
Gaithersburg, MD 20878

Lockheed Missiles and Space Co.
3251 Hanover St.
Bldg. 205, Dept 92-20
Palo Alto, CA 94304
Attn: Dr. John Siambis

Los Alamos National Laboratory
P.O. Box 1663
Los Alamos, NM 87545
Attn: Dr. L. Thode
Dr. H. Dogliani, MS-5000
Mr. R. Carlson, MS-P940
Dr. Carl Ekdahl, MS-D410
Dr. Joseph Mack
Dr. Melvin I. Buchwald
Dr. David C. Moir

Maxwell Laboratories Inc.
8888 Balboa Avenue
San Diego, CA 92123
Attn: Dr. Ken Whitham

McDonnell Douglas Research Laboratorie
Dept. 223, Bldg. 33, Level 45
Box 516
St. Louis, MO 63166
Attn: Dr. Carl Leader
Dr. Frank Bieniosek
Dr. John Honig

Mission Research Corporation
8560 Cinderbed Road
Suite 700
Newington, VA 22122
Attn: Dr. K. T. Nguyen

Mission Research Corporation
1720 Randolph Road, S.E.
Albuquerque, NM 87106
Attn: Dr. Thomas Hughes
Dr. Lawrence Wright
Dr. Kenneth Struve
Dr. Michael Mostrom
Dr. Dale Welch

Mission Research Corporation
P. O. Drawer 719
Santa Barbara, California 93102
Attn: Dr. C. Longmire
Dr. N. Carron

National Inst. of Standards & Tech.
Gaithersburg, Maryland 20760
Attn: Dr. Mark Wilson

Naval Postgraduate School
Physics Department (Code 61)
Monterey, CA 93940
Attn: Prof. John R. Neighbours
Prof. Fred Buskirk
Prof. Kai Woehler
Prof. Xavier Maruyama

Naval Surface Warfare Center
White Oak Laboratory
Code R-41
Silver Spring, Maryland 20903-5000
Attn: Mr. W. M. Hinckley
Dr. M. H. Cha
Dr. H. S. Uhm
Dr. R. Fiorito
Dr. R. Stark
Dr. H. C. Chen
Dr. D. Rule
Dr. Matt Brown
Mrs. Carolyn Fisher (G42)
Dr. Eugene E. Nolting (H23)

Office of Naval Research
800 North Quincy Street
Arlington, VA 22217
Attn: Dr. C. W. Roberson
Dr. F. Saalfeld

Office of Naval Research (2 copies)
Department of the Navy
Code 01231C
Arlington, VA 22217

Office of Under Secretary of Defense
Research and Engineering
Room 3E1034
The Pentagon
Washington, DC 20301
Attn: Dr. John MacCallum

Physics International, Inc.
2700 Merced Street
San Leandro, CA. 94577
Attn: Dr. E. Goldman
Dr. James Benford
Dr. George B. Frazier
Mr. Ralph Genuario

Pulse Sciences, Inc.
600 McCormack Street
San Leandro, CA 94577
Attn: Dr. Sidney Putnam
Dr. V. Bailey
Dr. M. Tiefenback

Pulse Sciences, Inc.
2001 Wilshire Boulevard
Suite 600
Santa Monica, CA 90403
Attn: Dr. John R. Bayless
Dr. R. Adler

The Rand Corporation
2100 M Street, NW
Washington, DC 20037
Attn: Dr. Nikita Wells
Mr. Simon Kassel

Sandia National Laboratory
Albuquerque, NM 87115
Attn: Dr. David Hasti/1272
Dr. Collins Clark
Dr. John Freeman/1241
Dr. Charles Frost
Dr. George Kamin/1274
Dr. Gordon T. Leifeste
Dr. Gerald N. Hays
Dr. Michael G. Mazarakis/1272
Dr. John Wagner/1241
Dr. Ron Lipinski/1274
Dr. James Poukey
Dr. Milton J. Clauser/1261
Dr. Kenneth R. Prestwich/1240
Dr. Kevin O'Brien
Dr. Isaac R. Shokair
Dr. J. Pace VanDevender/1200

Science Applications Intl. Corp.
5150 El Camino Road
Los Altos, CA 94022
Attn: Dr. R. R. Johnston
Dr. Leon Feinstein
Dr. Douglas Keeley
Dr. E. Roland Parkinson

Science Applications Intl. Corp.
1710 Goodridge Drive
McLean, VA 22102
Attn: Mr. W. Chadsey
Dr. A Drobot
Dr. K. Papadopoulos
Dr. William W. Rienstra
Dr. Alan J. Toepfer
Dr. Alfred Mondelli
Dr. D. Chernin
Dr. R. Tsang
Dr. J. Petillo

Science Research Laboratory, Inc.
1600 Wilson Boulevard
Suite 1200
Arlington, VA 22209
Attn: Dr. Joseph Mangano
Dr. Daniel Birx

Commander
Space & Naval Warfare Systems Command
PMW-145
Washington, DC 20363-5100
Attn: CAPT J. D. Fontana
LT Fritchie

Strategic Defense Initiative Org.
SDIO/T/DEO
The Pentagon
Washington, DC 20009-7100
Attn: Lt Col R. L. Gullickson
Dr. D. Duston

Titan/Spectron, Inc.
P. O. Box 4399
Albuquerque, NM 87196
Attn: Dr. R. Bruce Miller
Dr. John Smith

University of California
Physics Department
Irvine, CA 92664
Attn: Dr. Gregory Benford
Dr. Norman Rostoker

University of California
San Diego, CA 92110
Attn: Dr. Marshall N. Rosenbluth

UCLA
Physics Department
Los Angeles, CA 90024
Attn: Dr. F. Chen
Dr. C. Joshi
Dr. J. Dawson
Dr. N. Luhmann

University of Maryland
Physics Department
College Park, MD 20742
Attn: Dr. Y. C. Lee
Dr. C. Grebogi
Dr. W. Destler
Dr. C. Striffler
Dr. M. Reiser

University of Michigan
Dept. of Nuclear Engineering
Ann Arbor, MI 48109
Attn: Prof. Terry Kammash
Prof. R. Gilgenbach

Director of Research
U.S. Naval Academy
Annapolis, MD 21402 (2 copies)

Naval Research Laboratory
Washington, DC 20375-5000
Code 4830
Tim Calderwood